The First Quiescent Galaxies in TNG300

By

Abigail I. Hartley[1]

Advisor: Dr. Erica Nelson[1]

Committee: Dr. Bethany Wilcox[2], Dr. Mark Rast[1]

[1] Department of Astrophysical & Planetary Sciences

[2] Department of Physics

College of Arts & Sciences

University of Colorado Boulder

Oct. 31, 2023

TABLE OF CONTENTS

CHAPTER 1
INTRODUCTION AND BACKGROUND

By the time the Universe was 3 billion years old, half of its massive galaxies had stopped forming new stars [1, 2], but the variations in the time-scales and structural factors involved in their quenching processes often evade explanation. These quiescent galaxies appear to be unable to form stars because they lack reservoirs of cold, star-forming gas [3, 4, 1]. When observed at high redshifts, they are exceedingly compact [5, 6, 7, 8], which in principle allows for more expedient gas accretion onto their supermassive black holes (SMBHs). If a galaxy's central SMBH accretes rapidly enough, an active galactic nucleus (AGN) is formed, which serves as an incredibly luminous and persistent source of electromagnetic radiation [9, 10, 11]. By preventing further accumulation of cold gas and dust in the central regions of a galaxy [12, 13], AGN feedback is proposed to prohibit quiescent galaxies from rejuvenating and developing dense stellar cores later in time (but see also [14]). This feedback from early black holes has thus likely played a pivotal role in the quenching of early and massive galaxies [15, 16, 17], but causal evidence linking AGN feedback to quenching has been nearly impossible to establish observationally. This empirical uncertainty necessitates the use of cosmological simulations in studies of AGN feedback.

In the IllustrisTNG (hereafter TNG) cosmological simulation suite [18, 19] modeling galaxy formation, AGN feedback regulates black hole accretion and star formation with quasar-heating (thermal) and radio-jet (kinetic) wind modes, which work at different scales to expel cool star-forming gas from their host galaxies [20, 21]. The thermal mode heats surrounding gas within a galaxy, while the kinetic mode serves as a velocity boost to eject the gas. Both feedback modes may work in tandem to create and maintain the quiescence of their host galaxies at early cosmic times [22, 23].

Although many studies have been conducted to determine the physical properties and quenching processes of ancient quiescent galaxies [e.g., 24, 25, 26, 27], TNG provides a means to address

a cosmological enigma yet to be resolved in this field, namely the lives and quenching mechanisms of the very first quiescent galaxies in our Universe. The most massive galaxies in the Universe today host maximally old stars [e.g., 28, 29], suggesting that they are relics of very early star formation and the early truncation thereof. This empirical fact has naturally driven observational searches for the earliest progenitors of these systems, and examples of these massive, quiescent galaxies have been spectroscopically confirmed as early as $z \sim 4$ (~ 1.5 billion years after the Big Bang) [30, 31, 32]. However, the intrinsically red colours and high mass-to-light ratios of older stellar populations have rendered direct study of the earliest red-and-dead systems observationally out of reach prior to the vastly improved sensitivity, wavelength coverage, and resolution of the *JWST*. Early studies of the first *JWST* datasets have provided photometric candidates of the emerging population of quiescent galaxies [33], but the formation timescales of these sources remain uncertain. Furthermore, observational evidence connecting those galaxies to their ultimate descendant galaxies in the local Universe are fundamentally limited. Investigating the evolution and quenching processes of the first massive quiescent galaxies in the largest volume of the TNG simulation suite provides some theoretical underpinnings for the groundbreaking examinations of quiescent galaxies that observational missions like *JWST* will produce.

In this thesis, we shed light on the physical properties, star formation histories, quenching processes (AGN feedback modes), and evolution of the first galaxies to stop forming stars in the TNG300 simulation. The paper is organized as follows. In Section 2, we give a brief overview of the IllustrisTNG project and simulation utilized in this study. We then describe criteria for selection of the first quiescent galaxies within TNG300. In Section 3, we set forth our results regarding the first quenched galaxies identified in TNG, as well as critical information about their physical properties and star formation histories (Section 3.1). We then discuss the sample's evolution to $z = 0$ (Section 3.2) and explore the quenching mechanisms acting on these galaxies (Section 3.3). Section 4 briefly relays the final conclusions drawn from this work, including its applications to the *JWST* mission.

CHAPTER 2

METHODOLOGY

2.1 The TNG300 Simulation

This study utilizes simulations from the IllustrisTNG project [18, 34, 19, 35, 36, 37, 38]. TNG is a suite of cosmological magnetohydrodynamical simulations run using the moving-mesh AREPO code [39]. By solving the conservation laws of ideal hydrodynamics with a finite volume approach, AREPO has the automatic adaptivity of Lagrangian smoothed particle hydrodynamics, while also retaining the accuracy advantages of Eulerian mesh-based methods. TNG is an updated version of the model employed in the original Illustris Project [40, 41, 42, 43] and simulates galaxy formation physics with a hybrid multiphase model for quiescent star formation coupled with radiative heating and cooling, solving for the integrated evolution of cosmic gas, luminous stars, dark matter and SMBHs [44, 45]. The simulations include SMBH growth with high-accretion state thermal mode [46, 47, 20] and low-accretion state kinetic wind mode AGN feedback [48, 49]. The instantaneous SMBH mass accretion rates calculated by TNG reflect the expected Bondi accretion rate of each respective SMBH given its mass and the properties of the surrounding gas.

The TNG suite consists of three simulation boxes with varying resolutions and volumes, which allows for both narrow and extensive cosmological studies. Because we would like to study rare galaxies, we utilize data selected from the TNG300 simulation [50], which has has a box size of $\sim$ 300 Mpc^3, the largest volume of the TNG suite. The simulation assumes the [51] best fit cosmological parameters, namely a dark energy density $\Omega_\Lambda = 0.6911$, baryon density $\Omega_b = 0.0486$, matter density $\Omega_m = 0.3089$, Hubble constant $H_0 = 67.74$ km s^{-1} Mpc^{-1}, spectral index $n_s = 0.9667$, and normalization $\sigma_8 = 0.8159$. TNG300 evolves dark matter particles with mass of $6 \times 10^7 \mathrm{M}_\odot$ and baryonic elements (stellar particles and gas cells) with mass resolution of $1.1 \times 10^7 \mathrm{M}_\odot$.

TNG employs the SUBFIND algorithm [52, 53] to locate gravitationally bound structures

within the simulation. These structures include subhaloes and dark matter haloes, with associated baryonic components that comprise galaxies within each subhalo. Subhaloes are tracked through snapshots in time using SUBLINK merger trees [54]. A subhalo's descendant is the subhalo with the highest weighted sum of individual particles (gas, stars, and dark matter) shared with the progenitor. These particles are ranked by gravitational binding energy and weighted by (rank)$^{-1}$. A merger takes place when multiple subhaloes share a common descendant, and the main progenitor of this descendant is defined as whichever subhalo has the most massive history [55].

2.2 Sample Selection

We select galaxies that are quiescent by requiring specific star formation rate (sSFR), defined as star formation rate normalized by galaxy mass within twice the stellar half-mass radius (INRAD quantities in the TNG catalogues), to fall below 10^{-11} yr^{-1} [56, 57]. We check that the descendant subhaloes of our selection maintain quiescence down to $z = 2$, in order to exclude temporary low-activity galaxies and ensure that we are locating those that are truly quenched. Finally, we limit galaxy stellar mass M_* to $\log(\mathrm{M}_*/\mathrm{M}_\odot) > 10.5$. This restricts our search to subhaloes with stellar masses greater than 1000 times the baryonic mass resolution of TNG300-1, so that all galaxies are resolved with roughly 10^4 star particles. Limiting our study to highly resolved, massive sources allows us to more accurately assess the structures and evolution of the galaxies we select.

CHAPTER 3

RESULTS: THE FIRST QUIESCENT GALAXIES IN TNG300

The first quiescent galaxies in TNG300 emerge at $z \sim 4.2$, roughly 1.5 Gyr after the Big Bang. No snapshots in time prior to $z = 4.18$ contain galaxies that fit our criteria in the simulation. To ensure a robust selection, we experimented with a higher sSFR cut of $10^{-10}\mathrm{yr}^{-1}$, and our five selected galaxies were still the only quiescent candidates at $z = 4.18$ (with no new galaxies fitting these criteria at higher redshifts). Lowering our mass cut to $10^{10}\mathrm{M}_{\odot}$ resulted in the emergence of a new quiescent galaxy at the prior snapshot of $z = 4.43$, which was found to be a galaxy from our sample that hadn't yet reached its star formation peak. We also checked TNG50, the highest resolution simulation of the TNG suite, for galaxies meeting our original criteria, and found the first match to occur at $z = 3.0$ (mostly due to a volume effect). With a larger volume, we may detect even rarer quiescent sources at higher redshifts. We note that the TNG300 simulation's effective comoving area at $z \approx 4.2$ is roughly 75% of that covered by the five HST CANDELS survey fields at the same redshift [58]. By redshift $z = 5$, TNG300's effective comoving area only makes up $\sim 50\%$ of that of the CANDELS survey, which may indicate compelling discrepancies between observed and simulated samples of high-redshift quiescent galaxies.

Fig. 3.1 plots sSFR versus galaxy stellar mass for all subhaloes with $\mathrm{M}_{*} > 10^{8}\mathrm{M}_{\odot}$ at $z = 4.18$, displaying the clear locus of galaxies at sSFR $\sim 3 \times 10^{-9}$ which make up the star-forming main sequence (SFMS) [59]. However, 9% of galaxies fall > 1 dex below this main sequence. All five galaxies below an sSFR of 10^{-11} and above a stellar mass of $3 \times 10^{10}\mathrm{M}_{\odot}$ have already passed their star formation peaks.

We find the number density of our sample, defined as the number of galaxies that fit our selection criteria at $z \sim 4.2$ divided by the effective volume of the TNG300 simulated box, to be $n = 1.32 \times 10^{-5}\ \mathrm{Mpc}^{-3}$. This closely resembles the observational number densities calculated by [33] reflecting massive quiescent galaxies located by *JWST* at $3 < z < 5$, and by [60] in their study

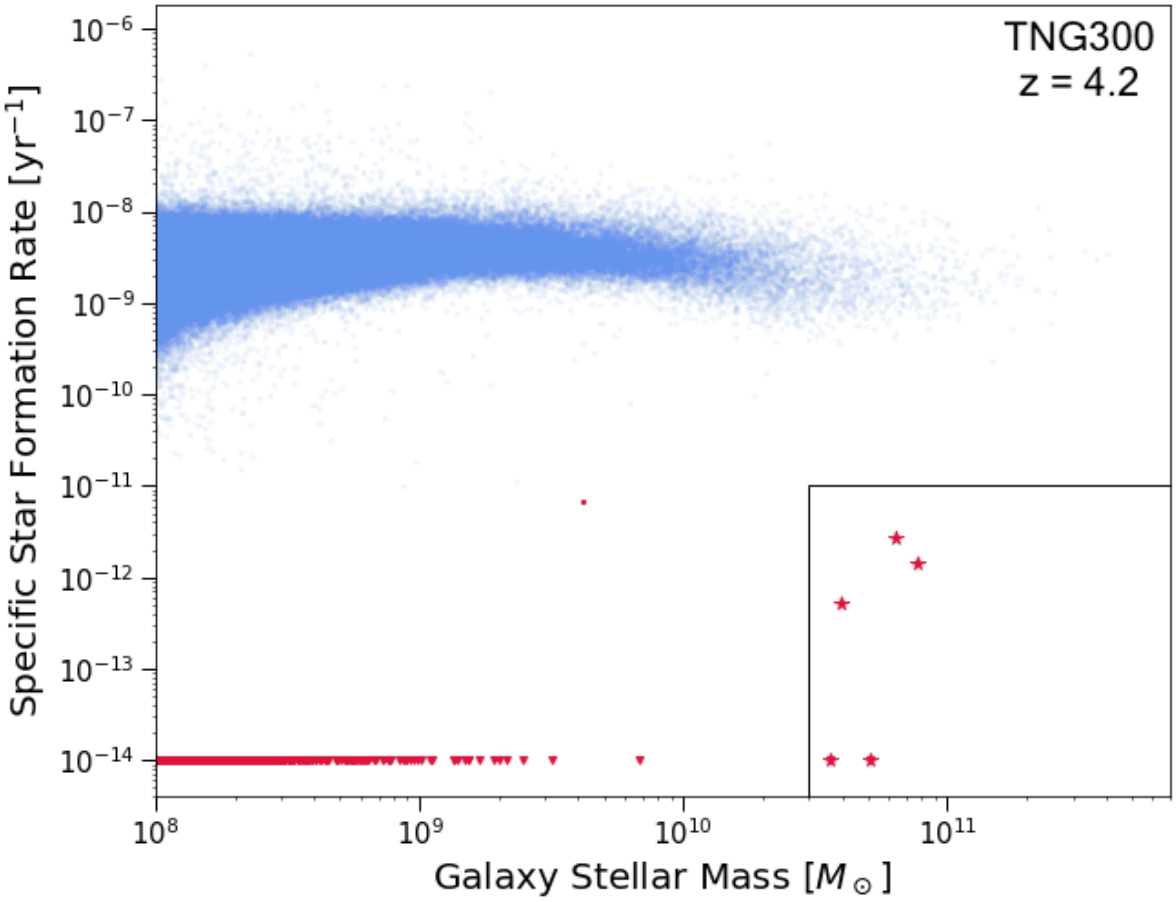

Figure 3.1: sSFR within twice the stellar half-mass radius of each galaxy with $\mathrm{M}_* > 10^8\mathrm{M}_\odot$ at $z = 4.18$ as a function of total stellar mass in the TNG300 simulation. Galaxies with sSFR $< 10^{-11}\mathrm{yr}^{-1}$ are colored red; all others are colored blue. Galaxies with sSFR$= 0$ have been brought up to the band at sSFR $= 10^{-14}$ [yr^{-1}] in downward carets. Galaxies with stellar masses below $10^8\mathrm{M}_\odot$ are not resolved and thus excluded from this visualization. Our selection criteria of massive quiescent galaxies is boxed; five galaxies satisfy this selection in TNG300 at $z \sim 4.2$.

of massive quiescent galaxies at $3 < z < 4$ identified in the ZFOURGE and 3DHST catalogues [61, 62]. The authors of [60] report a number density of $2.0 \pm 0.3 \times 10^5 n/\mathrm{Mpc}^3$ for a spectroscopic sample of quiescent galaxies at $3 < z < 4$, and the number density of quiescent galaxies in [33]'s robust sub-sample at $3 < z < 4$ is found to be $6.3^{+3.8}_{2.5} \times 10^5 n/\mathrm{Mpc}^{-3}$. [31] show that the number densities of these quiescent galaxies at $3 < z < 4$ are consistent between simulations and observations. Furthermore, the authors of [33] report a number density of $2.3^{+3.1}_{1.5} \times 10^5 n/\mathrm{Mpc}^3$ for massive quiescent galaxies located by *JWST* at $4 < z < 5$. However, these observed number densities of high-redshift quiescent galaxies are dependent upon measurement choices, such as definitions of quiescence and SFR time-scale, and sample selection functions, which impact their comparison to theoretical investigations [63]. The number densities presented in early *JWST* studies also reflect conservative lower limits from preliminary observations, which would benefit from further spectroscopic confirmation.

3.1 Physical Properties and Star Formation Histories

Fig. 3.2 plots the time evolution of the star formation rates of our selected galaxies, their stellar masses, black hole masses, gas masses, and stellar half-mass radii. These plots include all mergers experienced by our sample galaxies since $z = 4.18$, with a dashed line indicating that the galaxy merged into a more massive halo and is no longer its descendant's main progenitor. All galaxies are first identified as quiescent at an age of 1.47 Gyr after the Big Bang, marked in blue with a vertical line on each panel of the figure. This line illustrates that our galaxies of interest have indeed passed their epochs of peak star formation.

Our sample displays star formation rates that drop off and approach zero soon before an age of ~ 1.47 Gyr, with star formation history shapes defined by early peaks with compact widths. The average sSFR of this sample at $z = 4.18$ is $9.22 \times 10^{-13} \mathrm{yr}^{-1}$, which falls a few orders of magnitude below the sSFR associated with the SFMS at this redshift. We find that this sample experiences an expeditious quenching time-scale of ~ 0.35 Gyr. The duration of quenching is defined as the time period during which the sSFR drops continuously from its peak value to sSFR $= 1/[20 t_{\mathrm{H}}(z)]$,

where $t_{\rm H}(z)$ is the Hubble time at each redshift. This quenching is reflected as a decrease in the rate of stellar mass growth preceded by a rapid rise in black hole mass for each galaxy. The mass growth of these galaxies' SMBHs thus seems to be an integral driving factor in their quenching.

We find the average stellar mass contained within twice our sample's respective stellar half-mass radii at an age of 1.47 Gyr to be $5.39 \times 10^{10} \mathrm{M}_{\odot}$. In comparison, the average gas mass within the same radius for each galaxy is $1.82 \times 10^{8} \mathrm{M}_{\odot}$. We calculate the mean gas fraction of this sample over the span of its quenching era, ~ 1.11 Gyr to ~ 1.47 Gyr ($z = 5.23$ to 4.18), in order to gauge the rate at which gas depletion occurs within these galaxies. This fraction drops from 0.53 at $z = 5.23$ to 0.25 at $z = 4.43$, and finally to 3.39×10^{-3} at $z = 4.18$. This suggests that these quiescent galaxies very rapidly lose their gas while quenching, as expected for a sample with such low specific star formation rates [3, 4, 64]. These galaxies display an average gas-phase metallicity of $Z = 0.21 Z_{\odot}$.

The stellar half-mass radii of our sample range from 0.7 to 1.3 kpc when they are first identified as quiescent, which is standard for massive galaxies at $z = 4.18$ in TNG300; the average stellar half-mass radius for galaxies with $\mathrm{M}_{*} > 3 \times 10^{10} \mathrm{M}_{\odot}$ in the snapshot is a compact 1.29 kpc. Our five selected galaxies also display distinctly disk-like morphologies.

Utilizing stellar formation times from each star particle within each sample galaxy, we find that the oldest star within the first massive quiescent galaxies in TNG300 formed at a high redshift of $z = 15.1$. On average, however, the stars composing these galaxies were born at $z \approx 5.49$, which corresponds to a lookback time of ~ 12.7 Gyr. With an average stellar age of ~ 0.5 Gyr, this sample is consistent with observed post-starburst galaxies [65]; the first quiescent galaxies in TNG300 quenched quickly.

To explore how these objects would be detected in real surveys, we provide magnitude estimates in H160 and F444W, typical detection bands for the *Hubble Space Telescope* and *JWST*, respectively. We find the average apparent AB magnitude of our sample to be 24.6 in the U rest frame band, which is comparable to H160, and 23.7 in the i rest frame band, which is comparable to F444W detection limits. These magnitudes indicate that we have located a strong sample of

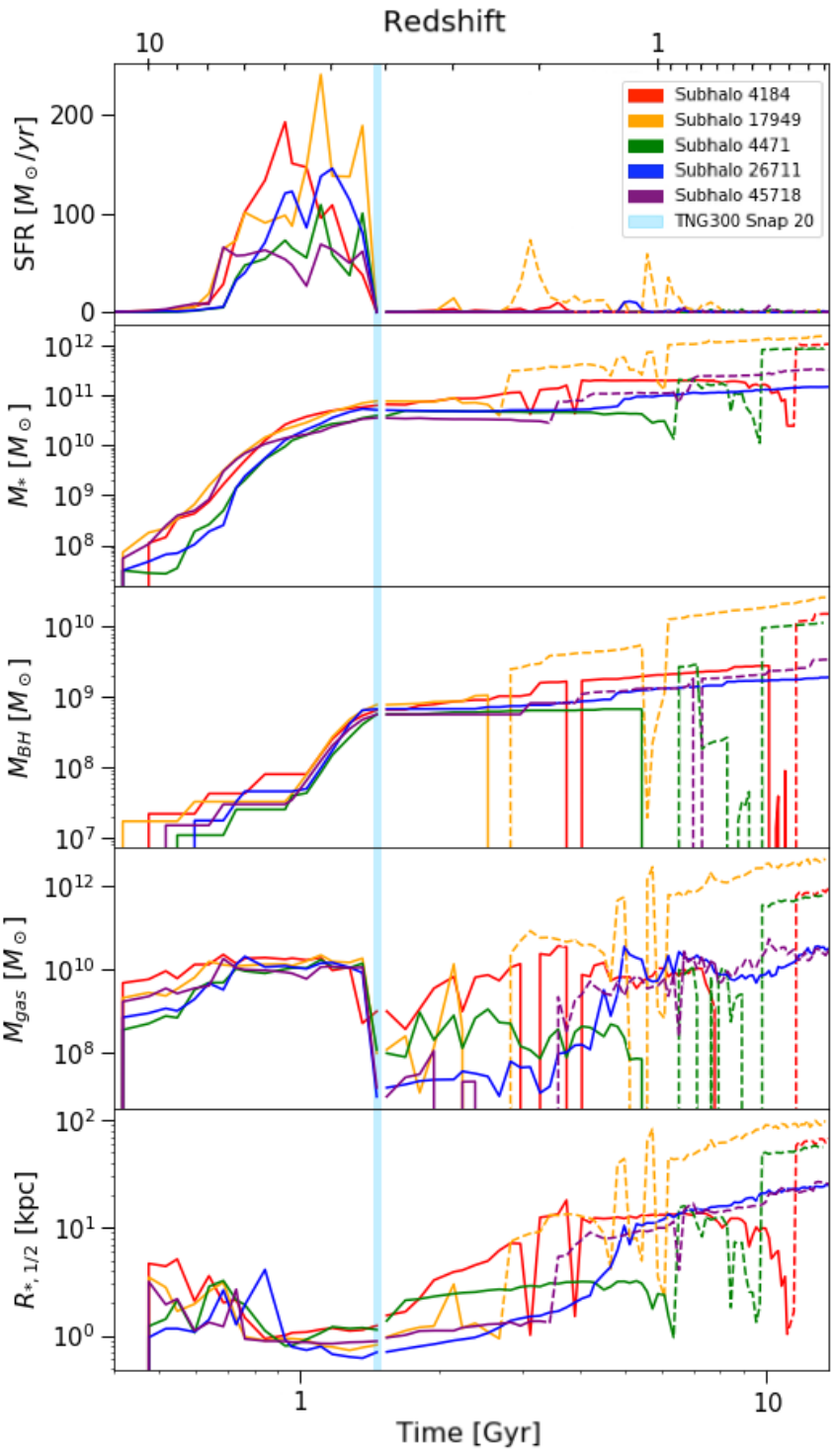

Figure 3.2: For each galaxy in our sample, this plot shows the time evolution of star formation rate (SFR), stellar mass (M_*), SMBH mass (M_{BH}), gas mass ($\mathrm{M}_{\mathrm{gas}}$), and stellar half-mass radius ($R_{*,1/2}$). All quantities are restricted to cells within twice the stellar half mass radius of each galaxy. An age of 1.47 Gyr is marked in light blue on each plot to indicate the time of study (Snapshot 20 of TNG300, or $z = 4.18$). After galaxies in the sample merge into more massive subhaloes, they are plotted with dashed lines.

simulated candidates to obtain *JWST* NIRSpec spectra for in the real Universe. The magnitudes also corroborate those reported in [66]. However, the TNG300 simulation does not account for extinction from dust, which may reduce the accuracy of these approximations. Quiescent galaxies generally have limited reserves of dust, but we should still expect a potential disparity of up to half a mag between our above estimates of apparent visual magnitude and the brightnesses of similar galaxies located in our Universe.

3.2 Evolution to $z = 0$

Contrary to initial expectations that the first quiescent galaxies in TNG would persist as the most central and massive galaxies of their respective haloes, we find that only one of our five selected galaxies lies on the main progenitor branch of its $z = 0$ descendant. The remaining four merge into other, more massive galaxies. This can be seen in Fig. 3.3, which juxtaposes complete merger tree diagrams generated by TNG for the evolutions of: (a) the only galaxy in the sample to lie on the main progenitor branch of its $z = 0$ descendant, and (b) through (e), the remaining galaxies in the sample which are far removed from their main progenitor branches.

The fact that our selected galaxies in the right four panels do not lie on this branch of the most massive galaxies leading up to their final $z = 0$ subhaloes, is a surprise. [67], for example, found that a mere 15 per cent of their selected massive compact quiescent galaxies in Illustris were consumed in mergers with more massive galaxies on their evolutionary paths from $z = 2$ to $z = 0$. The majority of galaxies in their sample instead either acquired ex situ envelopes to become the cores of more massive descendants, or survived undisturbed. [68] further describe a model wherein compact high-redshift galaxies comprise the centres of normal nearby ellipticals and grow via minor mergers, which predicts that these galaxies serve as the progenitors of massive elliptical galaxies in the local universe.

In order to explore the large-scale structural transformation of our sample of galaxies, we calculate their physical properties at redshift $z = 0$ and determine what they have become. At $z = 0$, the only galaxy in our sample to lie on the main progenitor branch of its $z = 0$ descendant sports

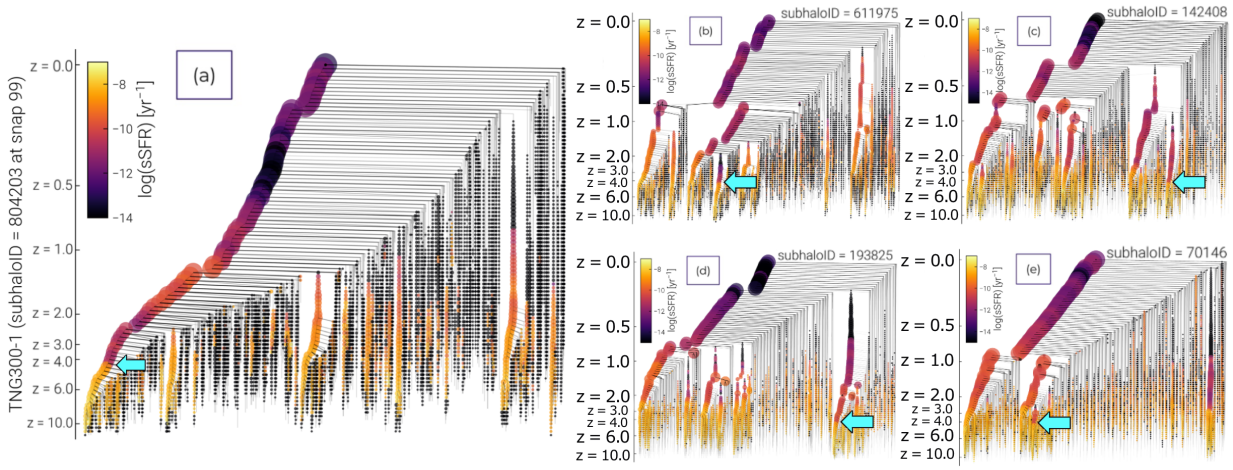

Figure 3.3: Complete merger trees for (a) the only galaxy in the sample to lie on the main progenitor branch of its $z = 0$ descendant and (b) through (e) the remaining galaxies in the sample. Cyan arrows indicate where our sample galaxies lie on these trees. TNG generates these diagrams by tracking all of the galaxies that have merged into the final galaxy at the top of the tree (at redshift $z = 0$). Galaxies are color coded according to logarithmic sSFR, and subhalo sizes are determined by stellar mass.

a stellar half-mass radius of ~ 24.5 kpc. The remaining galaxies in our sample have merged into larger galaxy clusters whose centrals have stellar half-mass radii ranging from 25 to 97 kpc. These radial measurements extend deep into the haloes of the clusters, and would thus make for poor comparisons to observational data.

After a galaxy in the sample merges into another more massive object, it is plotted with a dotted line in Fig. 3.2, which illustrates that a significant amount of this radial increase is due to major mergers into larger galaxy clusters. We find that the average stellar mass of our sample has increased to $7.94 \times 10^{11}\mathrm{M}_{\odot}$, and the associated average gas mass has increased to $1.13 \times 10^{12}\mathrm{M}_{\odot}$. Our results suggest that the first quiescent galaxies become brightest cluster galaxies (BCGs) in the local Universe at $z = 0$. Though the majority of our sample of galaxies are not the main progenitors of BCGs, they are likely the most massive galaxies contributing to the centres of these clusters.

3.3 Quenching Processes: SMBH Accretion and AGN Feedback

At $z \sim 4.2$, the SMBHs within our sample have just experienced rapid mass growth, as evidenced by the middle panel of Fig. 3.2. We quantify this accretion by calculating the average black hole growth rate between snapshots. From $z = 4.66$ to $z = 4.18$, a span of 0.18Gyr, our sample's central black holes grow by an average of $1.35 \times 10^9 \mathrm{M}_\odot/\mathrm{Gyr}$. We find the average black hole growth rate from $z = 4.18$ to $z = 0$, a span of 12.34Gyr, to have declined to stabilize at $4.92 \times 10^8 \mathrm{M}_\odot/\mathrm{Gyr}$, a phenomenon which may be explained by the regulatory nature of AGN feedback in relation to black hole mass.

Our sample's SMBHs exhibit thermal AGN feedback during the entire quenching era of these galaxies, $\sim$ 1.11 Gyr to $\sim$ 1.47 Gyr after the Big Bang. At $1.11\mathrm{Gyr}$, the kinetic energy injection feedback mode turns on in the simulation for the sole galaxy in our sample that is the main progenitor of its $z = 0$ descendant, and at $1.28\mathrm{Gyr}$ for the remaining galaxies in the sample.

To account for the potential role of stellar feedback in the quenching processes of our sample, we utilise feedback energy equations provided by [69]. We find that though thermal AGN and stellar feedback dominate at higher redshifts, these rates of feedback energy experience minimal growth during our sample's quenching epoch. Instead, it appears that quenching is largely driven by kinetic AGN feedback, which acts later to efficiently expel remaining reserves of star-forming gas. This corroborates [69]'s finding that kinetic AGN feedback tends to take over at late times in massive haloes in order to keep the star formation rate low. Fig. 3.4 displays that the onset of quenching at $z \sim 4.2$ in TNG300 takes place when kinetic mode energy exceeds 1 per cent of the thermal mode. The necessity of low-accretion state kinetic AGN feedback in the quenching processes of these galaxies is further substantiated by [49, 18, 70, 71, 59], who show that TNG galaxies quench only when the kinetic wind mode of feedback is turned on. This mode is more efficient in halting star formation in a host galaxy than the quasar-heating mode, as thermal energy produced by the latter is quickly radiated away. We conclude that AGN feedback has driven the quenching process of the galaxies in our sample. For each galaxy, rapid SMBH growth and activa-

tion of a kinetic feedback mode coincide with a steep decline in star formation rate, as evidenced by Fig. 3.2.

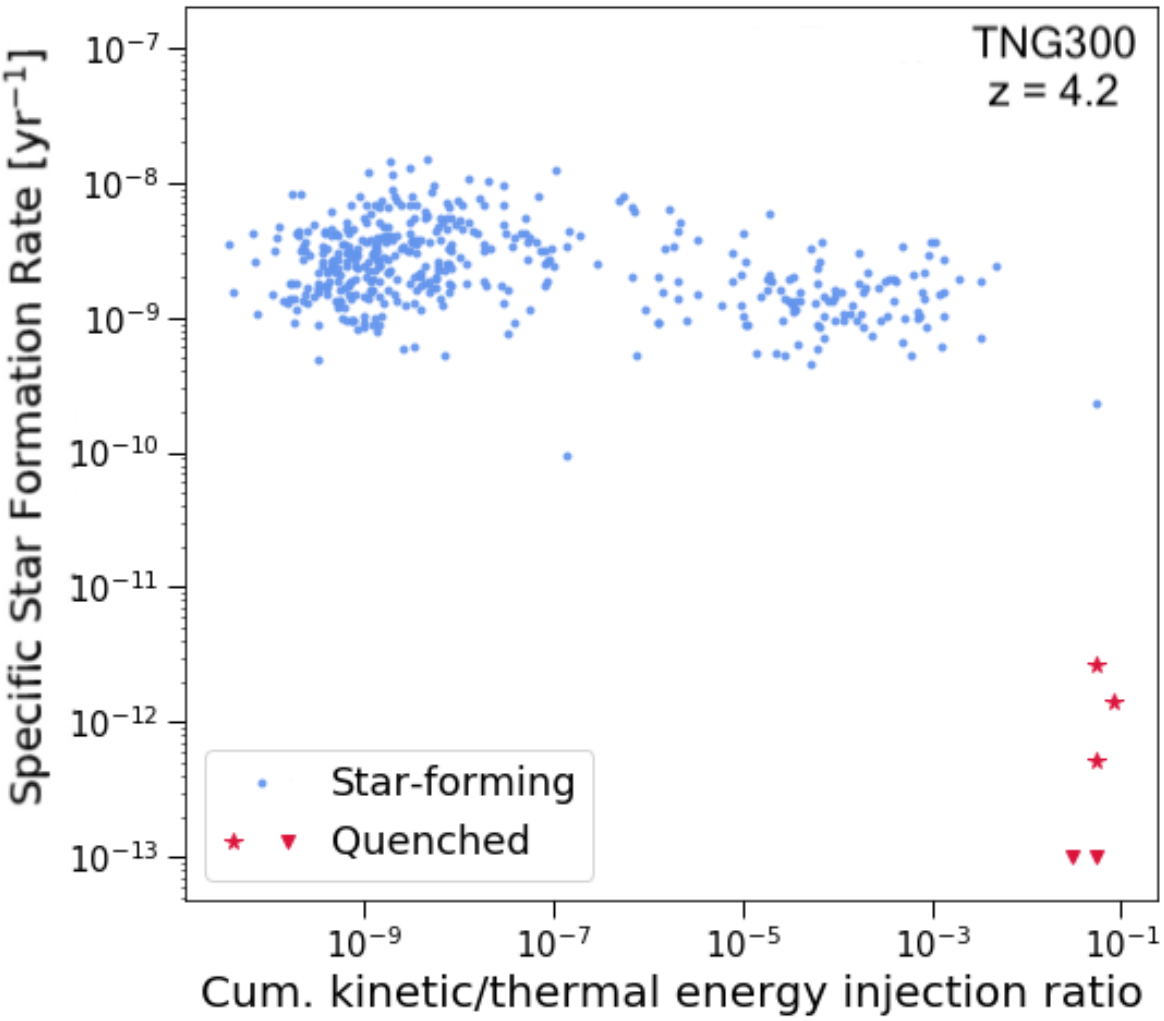

Figure 3.4: sSFR is plotted against the ratio between the cumulative energy injected by the kinetic and thermal AGN feedback modes to show the role of AGN feedback in setting the SFR of galaxies at $z \sim 4.2$ in TNG300. This includes our quiescent sample, along with all star-forming galaxies with $\mathrm{M}_* > 10^9 \mathrm{M}_\odot$. Galaxies with sSFR$= 0$ have been brought up to the band at sSFR $= 10^{-13}$ [yr^{-1}] in downward carets.

CHAPTER 4

CONCLUSIONS AND APPLICATIONS TO JAMES WEBB

We have studied the attributes and evolution of the first massive quiescent galaxies in the TNG300 simulation of the IllustrisTNG project. These galaxies' physical characteristics corroborate those of early massive quiescent galaxies directly observed in our Universe, namely a compact stellar half-mass radius and substantial stellar-to-gas mass ratio. However, our sample emphasises a critical evolutionary caveat: observed high-redshift quenched populations are far from the final word in the time evolution of the earliest quiescent galaxies. The truncation of star formation that is driven by AGN feedback in IllustrisTNG is only a pause in these developmental paths, which include significant growth and star formation in other branches of their evolutionary trees. While expanding our stellar mass and sSFR cuts to $10^{10}\mathrm{M}_{\odot}$ and 10^{-10} yr^{-1} did not yield additional TNG quiescent candidates, we intend to fully investigate quenching at lower mass regimes in future research.

With the results of this study, we predict that the first quiescent galaxies to be located by *JWST* will host massive black holes, and furthermore that the *JWST* mission will allow for spectroscopic confirmation of the presence of AGN at high redshifts ($4 < z < 5$). Additional noteworthy *JWST* predictions facilitated by TNG include the works of [72] and [73]. [72] provide predictions for the dust attenuation curves of high redshift galaxy populations ($z = 2 - 6$) based on the IllustrisTNG simulation suite, and the authors conclude that attenuation curves are steeper in galaxies at higher redshifts, with bluer colours, or with lower stellar masses. [73] present a catalogue of mock images of massive high-redshift galaxies from the TNG50 cosmological simulation. The authors analyse the predictions of TNG50 for the size evolution of galaxies at $3 \leq z \leq 6$ and the expectations for CEERS to probe that progression, finding a difference between the mass and light distribution, which may indicate a transition in the galaxy morphology at $z = 4-5$. *JWST* findings shall further test these predictions.

Furthermore, *JWST* has facilitated the selection of a sample of massive quiescent galaxies at

$3 < z < 5$ by [33]. The number density reported by the authors for massive quiescent galaxies at $4 < z < 5$, $n = 2.3^{+3.1}_{1.5} \times 10^5$ Mpc^3, is in agreement with the calculated number density of our sample, $n = 1.3 \times 10^5$ Mpc^3. This observational number density represents a conservative lower limit, indicating that *JWST* may reveal new insights into galaxy formation that will train the next generation of cosmological simulations. Our study serves as a strong test of the quenching mechanisms employed in such simulations; if larger samples of quiescent galaxies are observationally confirmed at higher redshifts than $z \sim 4.2$, as suggested by photometry [e.g., 74, 75], it implies an interesting discrepancy to pursue with further research of high-redshift galaxies.

REFERENCES

[1] K. E. Whitaker *et al.*, "Quenching of star formation from a lack of inflowing gas to galaxies,", vol. 597, no. 7877, pp. 485–488, Sep. 2021. arXiv: 2109.10384 [astro-ph.GA].

[2] A. Muzzin *et al.*, "The Evolution of the Stellar Mass Functions of Star-forming and Quiescent Galaxies to z = 4 from the COSMOS/UltraVISTA Survey,", vol. 777, no. 1, 18, p. 18, Nov. 2013. arXiv: 1303.4409 [astro-ph.CO].

[3] R. Bezanson *et al.*, "Extremely Low Molecular Gas Content in a Compact, Quiescent Galaxy at z = 1.522,", vol. 873, no. 2, L19, p. L19, Mar. 2019. arXiv: 1902.09564 [astro-ph.GA].

[4] C. C. Williams *et al.*, "ALMA Measures Rapidly Depleted Molecular Gas Reservoirs in Massive Quiescent Galaxies at z $\sim$ 1.5,", vol. 908, no. 1, 54, p. 54, Feb. 2021. arXiv: 2012.01433 [astro-ph.GA].

[5] P. G. van Dokkum, M. Kriek, and M. Franx, "A high stellar velocity dispersion for a compact massive galaxy at redshift z = 2.186,", vol. 460, no. 7256, pp. 717–719, Aug. 2009. arXiv: 0906.2778 [astro-ph.CO].

[6] P. Cassata *et al.*, "Constraining the Assembly of Normal and Compact Passively Evolving Galaxies from Redshift z = 3 to the Present with CANDELS,", vol. 775, no. 2, 106, p. 106, Oct. 2013. arXiv: 1303.2689 [astro-ph.CO].

[7] C. M. S. Straatman *et al.*, "The Sizes of Massive Quiescent and Star-forming Galaxies at z $\sim$ 4 with ZFOURGE and CANDELS,", vol. 808, no. 1, L29, p. L29, Jul. 2015. arXiv: 1506.01380 [astro-ph.GA].

[8] A. van der Wel *et al.*, "3D-HST+CANDELS: The Evolution of the Galaxy Size-Mass Distribution since z = 3,", vol. 788, no. 1, 28, p. 28, Jun. 2014. arXiv: 1404.2844 [astro-ph.GA].

[9] D. Irodotou *et al.*, "The effects of AGN feedback on the structural and dynamical properties of Milky Way-mass galaxies in cosmological simulations,", vol. 513, no. 3, pp. 3768–3787, Jul. 2022. arXiv: 2110.11368 [astro-ph.GA].

[10] C. M. Harrison, "Impact of supermassive black hole growth on star formation," *Nature Astronomy*, vol. 1, 0165, p. 0165, Jul. 2017. arXiv: 1703.06889 [astro-ph.GA].

[11] C. Harrison, "Impact of AGN on Massive Galaxy Evolution: Observational Signatures," in *Linking Galaxies from the Epoch of Initial Star Formation to Today*, Feb. 2019, 74, p. 74.

[12] E. Choi, R. S. Somerville, J. P. Ostriker, T. Naab, and M. Hirschmann, "The Role of Black Hole Feedback on Size and Structural Evolution in Massive Galaxies,", vol. 866, no. 2, 91, p. 91, Oct. 2018. arXiv: 1809.02143 [astro-ph.GA].

[13] A. Fluetsch *et al.*, "Cold molecular outflows in the local Universe and their feedback effect on galaxies,", vol. 483, no. 4, pp. 4586–4614, Mar. 2019. arXiv: 1805.05352 [astro-ph.GA].

[14] C. Woodrum *et al.*, "Molecular Gas Reservoirs in Massive Quiescent Galaxies at z 0.7 Linked to Late-time Star Formation,", vol. 940, no. 1, 39, p. 39, Nov. 2022. arXiv: 2210.03832 [astro-ph.GA].

[15] R. S. Beckmann *et al.*, "Cosmic evolution of stellar quenching by AGN feedback: clues from the Horizon-AGN simulation,", vol. 472, no. 1, pp. 949–965, Nov. 2017. arXiv: 1701.07838 [astro-ph.GA].

[16] M. Donnari *et al.*, "Quenched fractions in the IllustrisTNG simulations: the roles of AGN feedback, environment, and pre-processing,", vol. 500, no. 3, pp. 4004–4024, Jan. 2021. arXiv: 2008.00005 [astro-ph.GA].

[17] F. S. J. Nobels, J. Schaye, M. Schaller, Y. M. Bahé, and E. Chaikin, "The interplay between AGN feedback and precipitation of the intracluster medium in simulations of galaxy groups and clusters," *arXiv e-prints*, arXiv:2204.02205, arXiv:2204.02205, Apr. 2022. arXiv: 2204.02205 [astro-ph.GA].

[18] D. Nelson *et al.*, "First results from the IllustrisTNG simulations: the galaxy colour bimodality,", vol. 475, no. 1, pp. 624–647, Mar. 2018. arXiv: 1707.03395 [astro-ph.GA].

[19] A. Pillepich *et al.*, "First results from the IllustrisTNG simulations: the stellar mass content of groups and clusters of galaxies,", vol. 475, no. 1, pp. 648–675, Mar. 2018. arXiv: 1707.03406 [astro-ph.GA].

[20] D. Sijacki, V. Springel, T. Di Matteo, and L. Hernquist, "A unified model for AGN feedback in cosmological simulations of structure formation,", vol. 380, no. 3, pp. 877–900, Sep. 2007. arXiv: 0705.2238 [astro-ph].

[21] S. Murthy *et al.*, "Cold gas removal from the centre of a galaxy by a low-luminosity jet," *Nature Astronomy*, vol. 6, pp. 488–495, Feb. 2022. arXiv: 2202.05222 [astro-ph.GA].

[22] R. Morganti, "The many routes to AGN feedback," *Frontiers in Astronomy and Space Sciences*, vol. 4, 42, p. 42, Nov. 2017. arXiv: 1712.05301 [astro-ph.GA].

[23] S. Cielo, R. Bieri, M. Volonteri, A. Y. Wagner, and Y. Dubois, "AGN feedback compared: jets versus radiation,", vol. 477, no. 1, pp. 1336–1355, Jun. 2018. arXiv: 1712.03955 [astro-ph.GA].

[24] P. G. van Dokkum *et al.*, "Forming Compact Massive Galaxies,", vol. 813, no. 1, 23, p. 23, Nov. 2015. arXiv: 1506.03085 [astro-ph.GA].

[25] M. Park *et al.*, "On the formation of massive quiescent galaxies with diverse morphologies in the TNG50 simulation," *arXiv e-prints*, arXiv:2112.07679, arXiv:2112.07679, Dec. 2021. arXiv: 2112.07679 [astro-ph.GA].

[26] J. Zhang *et al.*, "3D intrinsic shapes of quiescent galaxies in observations and simulations,", vol. 513, no. 4, pp. 4814–4832, Jul. 2022. arXiv: 2204.10867 [astro-ph.GA].

[27] P. Lustig *et al.*, "Massive quiescent galaxies at $z \sim 3$: a comparison of selection, stellar population and structural properties with simulation predictions," *arXiv e-prints*, arXiv:2201.09068, arXiv:2201.09068, Jan. 2022. arXiv: 2201.09068 [astro-ph.GA].

[28] D. Thomas, C. Maraston, K. Schawinski, M. Sarzi, and J. Silk, "Environment and self-regulation in galaxy formation,", vol. 404, no. 4, pp. 1775–1789, Jun. 2010. arXiv: 0912.0259 [astro-ph.CO].

[29] R. M. McDermid *et al.*, "The ATLAS^{3D} Project - XXX. Star formation histories and stellar population scaling relations of early-type galaxies,", vol. 448, no. 4, pp. 3484–3513, Apr. 2015. arXiv: 1501.03723 [astro-ph.GA].

[30] K. Glazebrook *et al.*, "A massive, quiescent galaxy at a redshift of 3.717,", vol. 544, no. 7648, pp. 71–74, Apr. 2017. arXiv: 1702.01751 [astro-ph.GA].

[31] F. Valentino *et al.*, "Quiescent Galaxies 1.5 Billion Years after the Big Bang and Their Progenitors,", vol. 889, no. 2, 93, p. 93, Feb. 2020. arXiv: 1909.10540 [astro-ph.GA].

[32] B. Forrest *et al.*, "The Massive Ancient Galaxies at z ¿ 3 NEar-infrared (MAGAZ3NE) Survey: Confirmation of Extremely Rapid Star Formation and Quenching Timescales for Massive Galaxies in the Early Universe,", vol. 903, no. 1, 47, p. 47, Nov. 2020. arXiv: 2009.07281 [astro-ph.GA].

[33] A. C. Carnall *et al.*, "A first look at JWST CEERS: massive quiescent galaxies from 3 ¡ z ¡ 5," *arXiv e-prints*, arXiv:2208.00986, arXiv:2208.00986, Aug. 2022. arXiv: 2208.00986 [astro-ph.GA].

[34] V. Springel *et al.*, "First results from the IllustrisTNG simulations: matter and galaxy clustering,", vol. 475, no. 1, pp. 676–698, Mar. 2018. arXiv: 1707.03397 [astro-ph.GA].

[35] J. P. Naiman *et al.*, "First results from the IllustrisTNG simulations: a tale of two elements - chemical evolution of magnesium and europium,", vol. 477, no. 1, pp. 1206–1224, Jun. 2018. arXiv: 1707.03401 [astro-ph.GA].

[36] F. Marinacci *et al.*, "First results from the IllustrisTNG simulations: radio haloes and magnetic fields,", vol. 480, no. 4, pp. 5113–5139, Nov. 2018. arXiv: 1707.03396 [astro-ph.CO].

[37] A. Pillepich *et al.*, "First results from the TNG50 simulation: the evolution of stellar and gaseous discs across cosmic time,", vol. 490, no. 3, pp. 3196–3233, Dec. 2019. arXiv: 1902.05553 [astro-ph.GA].

[38] D. Nelson *et al.*, "First results from the TNG50 simulation: galactic outflows driven by supernovae and black hole feedback,", vol. 490, no. 3, pp. 3234–3261, Dec. 2019. arXiv: 1902.05554 [astro-ph.GA].

[39] V. Springel, "E pur si muove: Galilean-invariant cosmological hydrodynamical simulations on a moving mesh,", vol. 401, no. 2, pp. 791–851, Jan. 2010. arXiv: 0901.4107 [astro-ph.CO].

[40] M. Vogelsberger, S. Genel, D. Sijacki, P. Torrey, V. Springel, and L. Hernquist, "A model for cosmological simulations of galaxy formation physics,", vol. 436, no. 4, pp. 3031–3067, Dec. 2013. arXiv: 1305.2913 [astro-ph.CO].

[41] M. Vogelsberger *et al.*, "Introducing the Illustris Project: simulating the coevolution of dark and visible matter in the Universe,", vol. 444, no. 2, pp. 1518–1547, Oct. 2014. arXiv: 1405.2921 [astro-ph.CO].

[42] M. Vogelsberger *et al.*, "Properties of galaxies reproduced by a hydrodynamic simulation,", vol. 509, no. 7499, pp. 177–182, May 2014. arXiv: 1405.1418 [astro-ph.CO].

[43] S. Genel *et al.*, "Introducing the Illustris project: the evolution of galaxy populations across cosmic time,", vol. 445, no. 1, pp. 175–200, Nov. 2014. arXiv: 1405.3749 [astro-ph.CO].

[44] V. Springel and L. Hernquist, "Cosmological smoothed particle hydrodynamics simulations: a hybrid multiphase model for star formation,", vol. 339, no. 2, pp. 289–311, Feb. 2003. arXiv: astro-ph/0206393 [astro-ph].

[45] A. Pillepich *et al.*, "Simulating galaxy formation with the IllustrisTNG model,", vol. 473, no. 3, pp. 4077–4106, Jan. 2018. arXiv: 1703.02970 [astro-ph.GA].

[46] T. Di Matteo, V. Springel, and L. Hernquist, "Energy input from quasars regulates the growth and activity of black holes and their host galaxies,", vol. 433, no. 7026, pp. 604–607, Feb. 2005. arXiv: astro-ph/0502199 [astro-ph].

[47] V. Springel, T. Di Matteo, and L. Hernquist, "Modelling feedback from stars and black holes in galaxy mergers,", vol. 361, no. 3, pp. 776–794, Aug. 2005. arXiv: astro-ph/0411108 [astro-ph].

[48] D. Sijacki *et al.*, "The Illustris simulation: the evolving population of black holes across cosmic time,", vol. 452, no. 1, pp. 575–596, Sep. 2015. arXiv: 1408.6842 [astro-ph.GA].

[49] R. Weinberger *et al.*, "Simulating galaxy formation with black hole driven thermal and kinetic feedback,", vol. 465, no. 3, pp. 3291–3308, Mar. 2017. arXiv: 1607.03486 [astro-ph.GA].

[50] D. Nelson *et al.*, "The IllustrisTNG simulations: public data release," *Computational Astrophysics and Cosmology*, vol. 6, no. 1, 2, p. 2, May 2019. arXiv: 1812.05609 [astro-ph.GA].

[51] Planck Collaboration *et al.*, "Planck 2015 results. XIII. Cosmological parameters,", vol. 594, A13, A13, Sep. 2016. arXiv: 1502.01589 [astro-ph.CO].

[52] V. Springel, S. D. M. White, G. Tormen, and G. Kauffmann, "Populating a cluster of galaxies - I. Results at [formmu2]z=0,", vol. 328, no. 3, pp. 726–750, Dec. 2001. arXiv: astro-ph/0012055 [astro-ph].

[53] K. Dolag, S. Borgani, G. Murante, and V. Springel, "Substructures in hydrodynamical cluster simulations,", vol. 399, no. 2, pp. 497–514, Oct. 2009. arXiv: 0808.3401 [astro-ph].

[54] V. Rodriguez-Gomez *et al.*, "The merger rate of galaxies in the Illustris simulation: a comparison with observations and semi-empirical models,", vol. 449, no. 1, pp. 49–64, May 2015. arXiv: 1502.01339 [astro-ph.GA].

[55] G. De Lucia and J. Blaizot, "The hierarchical formation of the brightest cluster galaxies,", vol. 375, no. 1, pp. 2–14, Feb. 2007. arXiv: astro-ph/0606519 [astro-ph].

[56] J. Brinchmann and R. S. Ellis, "The Mass Assembly and Star Formation Characteristics of Field Galaxies of Known Morphology,", vol. 536, no. 2, pp. L77–L80, Jun. 2000. arXiv: astro-ph/0005120 [astro-ph].

[57] R. Guzmán *et al.*, "The Nature of Compact Galaxies in the Hubble Deep Field. II. Spectroscopic Properties and Implications for the Evolution of the Star Formation Rate Density of the Universe1,", vol. 489, no. 2, pp. 559–572, Nov. 1997. arXiv: astro-ph/9704001 [astro-ph].

[58] N. Chartab *et al.*, "Large-scale Structures in the CANDELS Fields: The Role of the Environment in Star Formation Activity,", vol. 890, no. 1, 7, p. 7, Feb. 2020. arXiv: 1912.04890 [astro-ph.GA].

[59] E. J. Nelson *et al.*, "Spatially resolved star formation and inside-out quenching in the TNG50 simulation and 3D-HST observations,", vol. 508, no. 1, pp. 219–235, Nov. 2021. arXiv: 2101.12212 [astro-ph.GA].

[60] C. Schreiber *et al.*, "Near infrared spectroscopy and star-formation histories of $3 \leq z \leq 4$ quiescent galaxies,", vol. 618, A85, A85, Oct. 2018. arXiv: 1807.02523 [astro-ph.GA].

[61] R. E. Skelton *et al.*, "3D-HST WFC3-selected Photometric Catalogs in the Five CANDELS/3D-HST Fields: Photometry, Photometric Redshifts, and Stellar Masses,", vol. 214, no. 2, 24, p. 24, Oct. 2014. arXiv: 1403.3689 [astro-ph.GA].

[62] C. M. S. Straatman *et al.*, "The FourStar Galaxy Evolution Survey (ZFOURGE): Ultraviolet to Far-infrared Catalogs, Medium-bandwidth Photometric Redshifts with Improved Accuracy, Stellar Masses, and Confirmation of Quiescent Galaxies to z $\sim$ 3.5,", vol. 830, no. 1, 51, p. 51, Oct. 2016. arXiv: 1608.07579 [astro-ph.GA].

[63] M. Donnari, A. Pillepich, D. Nelson, F. Marinacci, M. Vogelsberger, and L. Hernquist, "Quenched fractions in the IllustrisTNG simulations: comparison with observations and other theoretical models,", vol. 506, no. 4, pp. 4760–4780, Oct. 2021. arXiv: 2008.00004 [astro-ph.GA].

[64] K. E. Whitaker *et al.*, "High Molecular-gas to Dust Mass Ratios Predicted in Most Quiescent Galaxies,", vol. 922, no. 2, L30, p. L30, Dec. 2021. arXiv: 2111.05349 [astro-ph.GA].

[65] K. A. Suess *et al.*, "{Squigg}ěc{l}{e} : studying quenching in intermediate-z galaxies-gas, {angu}ěc{l}{ar} momentum, and evolution,", vol. 926, no. 1, 89, p. 89, Feb. 2022. arXiv: 2111.14878 [astro-ph.GA].

[66] A. C. Carnall *et al.*, "A massive quiescent galaxy at redshift 4.658," *arXiv e-prints*, arXiv:2301.11413, arXiv:2301.11413, Jan. 2023. arXiv: 2301.11413 [astro-ph.GA].

[67] S. Wellons *et al.*, "The diverse evolutionary paths of simulated high-z massive, compact galaxies to z = 0,", vol. 456, no. 1, pp. 1030–1048, Feb. 2016. arXiv: 1507.02291 [astro-ph.GA].

[68] R. Bezanson *et al.*, "The Relation Between Compact, Quiescent High-redshift Galaxies and Massive Nearby Elliptical Galaxies: Evidence for Hierarchical, Inside-Out Growth,", vol. 697, no. 2, pp. 1290–1298, Jun. 2009. arXiv: 0903.2044 [astro-ph.CO].

[69] R. Weinberger *et al.*, "Supermassive black holes and their feedback effects in the IllustrisTNG simulation,", vol. 479, no. 3, pp. 4056–4072, Sep. 2018. arXiv: 1710.04659 [astro-ph.GA].

[70] B. A. Terrazas *et al.*, "The relationship between black hole mass and galaxy properties: examining the black hole feedback model in IllustrisTNG,", vol. 493, no. 2, pp. 1888–1906, Apr. 2020. arXiv: 1906.02747 [astro-ph.GA].

[71] E. Zinger *et al.*, "Ejective and preventative: the IllustrisTNG black hole feedback and its effects on the thermodynamics of the gas within and around galaxies,", vol. 499, no. 1, pp. 768–792, Nov. 2020. arXiv: 2004.06132 [astro-ph.GA].

[72] X. Shen *et al.*, "High-redshift JWST predictions from IllustrisTNG: II. Galaxy line and continuum spectral indices and dust attenuation curves,", vol. 495, no. 4, pp. 4747–4768, Jul. 2020. arXiv: 2002.10474 [astro-ph.GA].

[73] L. Costantin *et al.*, "Expectations of the size evolution of massive galaxies at $3 \leq z \leq 6$ from the TNG50 simulation: the CEERS/JWST view," *arXiv e-prints*, arXiv:2208.00007, arXiv:2208.00007, Jul. 2022. arXiv: 2208.00007 [astro-ph.GA].

[74] E. Merlin *et al.*, "Red and dead CANDELS: massive passive galaxies at the dawn of the Universe,", vol. 490, no. 3, pp. 3309–3328, Dec. 2019. arXiv: 1909.07996 [astro-ph.GA].

[75] A. Shahidi *et al.*, "Selection of Massive Evolved Galaxies at $3 \leq$ z ≤ 4.5 in the CANDELS Fields,", vol. 897, no. 1, 44, p. 44, Jul. 2020. arXiv: 2005.12507 [astro-ph.GA].